



Open Archive Toulouse Archive Ouverte (OATAO)

OATAO is an open access repository that collects the work of some Toulouse researchers and makes it freely available over the web where possible.

This is an author's version published in: <https://oatao.univ-toulouse.fr/28400>

Official URL : <https://doi.org/10.2514/6.2021-1059>

To cite this version :

Fayez, Karim and Leng, Yuchen and Jardin, Thierry and Bronz, Murat and Moschetta, Jean-Marc Conceptual Design for Long-Endurance Convertible Unmanned Aerial System. (2021) In: AIAA Scitech 2021 Forum, 11 January 2021 - 21 January 2021 (Virtual event, United States).

Any correspondence concerning this service should be sent to the repository administrator:

tech-oatao@listes-diff.inp-toulouse.fr

Conceptual Design for Long-Endurance Convertible Unmanned Aerial System

Karim Fayez ^{*} Yuchen Leng [†] Murat Bronz [‡] Thierry Jardin [§]
and Jean-Marc Moschetta [¶]
ISAE-SUPAERO, Université de Toulouse, France
ENAC, Toulouse, France
Delair, Labège, France

This research is aimed at analysing the effect of design parameters on critical aerodynamic performance of convertible unmanned aerial vehicle (UAV) with vertical take-off and landing (VTOL) capabilities and providing a sizing tool for its conceptual design. The research was based on new aerodynamic models specifically developed and validated for convertible aircraft, performed using mission-based optimisation techniques.

To accommodate a wide range of convertible aircraft configurations, a non-linear lifting-line method was used to efficiently analyse different combinations of lifting surface and propeller arrangements. Propeller loads were calculated using a blade element momentum approach and corrected for high incidence angle conditions according to numerical and experimental studies. Propeller-wing interactions were considered by modifying local boundary conditions at wing sections immersed in propeller slipstream.

Previous studies have suggested that the design of convertible aircraft is sensitive to typical mission requirements, notably the endurance breakdown between near-hover flight and cruise flight. A clear sizing law for wing and propeller according to given mission specification could greatly improve the understanding of compromises between hover and high speed flight.

I. Introduction

A. Background

The simplicity and compactness of unmanned aerial system (UAS) has lead to its increasing application in surveillance, delivery and mapping missions. The UAS family is mainly divided into two categories: fixed-wing and VTOL (Vertical Take-Off and Landing). While fixed wing vehicles are energy efficient, they can be deployed from a runway, a catapult or launched by hand. However all of these options require infrastructures and/or trained personnel, and thus there exists the need to reduce UAS field requirement during launch and recovery to further simplify the deployment of UAS. Such need inspired studies on aircraft capable of vertical take-off and landing. While VTOL vehicles can be launched in confined environment, typical designs suffer from poor energy efficiency. The interest of this project is then in the UAVs that combine VTOL capabilities with fixed wing capabilities, known as convertible UAVs.



(a) RWTH Aachen Tilt-Wing [1]



(b) ISAE MAVION [2]



(c) ENAC Cyclone [3]

Fig. 1 Convertible aircraft concepts

Traditionally, vertical take-off and landing operations were performed by rotorcraft such as helicopters. While suitable for small range missions, reduced rotor aerodynamic efficiency during forward flight limited aircraft range

and endurance performance. Development of a convertible aircraft that has comparable cruise efficiency to fixed-wing aircraft has long attracted attention from aeronautics community [4]. Several different configurations have been studied as shown in Figure 1. Tilt-rotor or tilt-wing design (Figure 1a) using additional servo to rotate propellers during transition flight to transform horizontal thrust towards vertical lift. A tailsitter design (Figure 1b, 1c) however uses aerodynamic control surfaces to achieve similar goal and thus is typically lighter and simpler for comparable tasks. The various configurations have different advantages and disadvantages so that careful analysis must be taken during conceptual design of a convertible UAV.

The goal of the project is to conduct a rigorous assessment on different convertible UAV configurations over different mission profiles. Current studies typically emphasis characteristics on a specific design, but a comprehensive study discussing how mission profile affects design choices is lacking. To achieve this goal, a multidisciplinary optimization tool is being developed based on OpenMDAO library [5] to perform the preliminary aerodynamic design of a convertible drone. The final methodology should be able to optimize several convertible UAV configurations and then compare them in terms of energy requirements for different flight phases. The tool will go through a series of optimization iterations taking into account important parameters such as the lifting surfaces and propulsive groups to ultimately design the most energy efficient configuration. This is to allow objective and quantifiable comparison between configurations, and thus promote further understanding on flight physics involved in VTOL aircraft.

B. State of the Art

This literature review attempts to identify, among the past significant studies on convertible UAV, the scope of possible configurations, the involved disciplines in design optimization and their level of fidelity, and finally the formulation of the optimization problem.

1. Mass and Balance

In a review conducted by Papageorgiou et al. on the advancements in MDO of aerial vehicles [6] it has been shown that the mass estimation discipline is the second most common discipline when it comes to aerial vehicles design. This is evident since vehicle mass is pivotal to the aerodynamic and performance calculations, which will ultimately be one of the most influential variables in the optimization [7].

For a preliminary design, it is acceptable to use a low-fidelity mass model for the optimization using empirical formulas, statistical data and mass models whenever possible. This reduces time during mass estimation instead of using costly high-fidelity models such as data from CAD. Moreover review from Papageorgiou has shown that 77% of the aerial vehicle MDO use low fidelity mass models [6].

The mass estimation will be done by breaking down the UAV into components and estimating each of their mass. We define the total mass of the vehicle as follows:

$$m_{\text{total}} = m_{\text{payload}} + m_{\text{structure}} + m_{\text{energy}} + m_{\text{propulsion}} \quad (1)$$

The detailed mass breakdown is as follows:

- m_{payload} : avionics and/or miscellaneous payload.
- $m_{\text{structure}}$: lifting surfaces and fuselage structure.
- m_{energy} : battery or fuel cell system mass.
- $m_{\text{propulsion}}$: propulsive group containing electric motors, electronic speed controllers and propellers.

As will be specified in section II.B, empirical formulae are used for the propeller based on the diameter, chord of and material density of the propeller. For the ESC and motors a linear model based on certain parameters of the components such as amperage rating or dimensions is developed. For the batteries an empirical formula based on the specific energy consumption of the battery. For the non-lifting surfaces such as fuselage or nacelle, a volumetric approach with the density of the material is used to estimate the weight. For the lifting surfaces such as the wings, a formula based on a volumetric approach of the components of the wing is used.

2. Structural Analysis

Papageorgiou et al. also found that the structural analysis was present in 66% of the studies and was the third most common discipline [6]. In the context of the current optimization problem, the structural analysis is chosen to be applied only to the wing spars, to ensure the structural integrity of the wing in the most severe flight conditions defined by maximal normal load factor. This is done by sizing the spar to withstand the required constraints. Moreover it allows

increases mass estimation fidelity, since the mass of spar is fed back to mass model. The structural model is simplified to a low fidelity model, consisting a cantilever beam under elliptical load distribution. The details of the model are presented in Section II.C. In future applications the outputs of this simple structural model could be used to allow more complex dynamic aeroelastic computations.

3. Aerodynamics and Stability

In the same review done by Papageorgiou et al. [6], they found that 52% of the aerodynamics models used in MDO were reduced order models (Panel codes), 11% medium resolution (Euler Solvers or coarse CFD simulations) and 37% high resolution (Full CFD simulation).

The wide use of reduced order models is a practical choice. In the preliminary design phase, large combination of design variables is necessary, which requires robust and efficient algorithms. On the other hand, the goal of preliminary design is to obtain general aircraft size while neglecting configuration details and thus the requirement on accuracy can be relaxed. Furthermore when considering the aerodynamics of a convertible UAV, there are very different flight conditions that the aircraft will encounter from the VTOL phase, through transition, to horizontal flight. As mentioned before, such aerodynamic tool box must be able to handle unusual attitude and different combinations of propulsion and lifting surface combinations. Computational cost and time required for high resolution model to analyse these conditions are usually undesired in this design stage. In conclusion, the choice of using reduced order models is a compromise of computational cost, robustness and the requirement of precision.

The enhanced Machup library [8, 9] is such a suitable low-fidelity aerodynamic model. The model has been validated at ISAE [10], and it has been improved to take into account high-angle of attack computations, based on findings from the dedicated wind tunnel experiment. This allows more accurate aerodynamic estimation at a still affordable computational cost.

4. Electric Propulsion

For the current application, electric propulsion is the selected method of propulsion. In most applications of UAVs above 100g brushless DC motors are used [11]. A propulsion group is defined to consist of: a propeller, a motor, an electric speed controller (ESC). The propulsion group is presented in Fig. 2, where the set point from the flight controller is the input to the group, and thrust is the output.

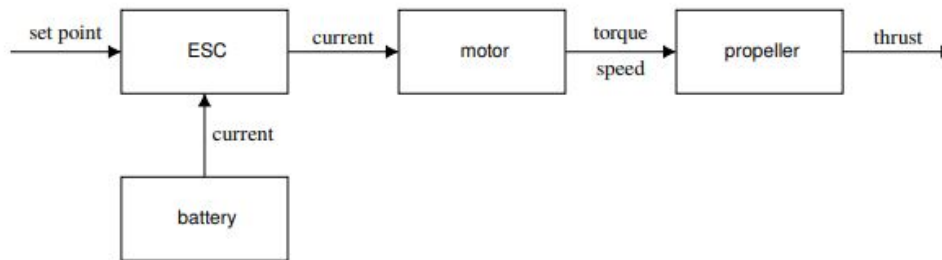


Fig. 2 Multicopter Propulsion Group [11]

In the context of this optimization, the electric propulsion optimization would be advantageous to have since there exists a multitude of propulsion groups in VTOL UAVs. This optimization can be achieved by performing propeller-motor matching. This concept revolves around finding the optimal efficiency for a combination of a motor and propeller for a given flight mission. QPOPTIMIZER is a tool developed for this specific purpose [12]. It has two main capabilities. The first one is matching the most appropriate motor and propeller combination for defined mission requirements. This is based on a database of propellers and motors. The second capability is designing the best propeller using a match from the motor database. The workflow of QPOPTIMIZER is presented in Figure 3.

However for the current optimization problem, QPOPTIMIZER has not been implemented yet and is planned for in future work.

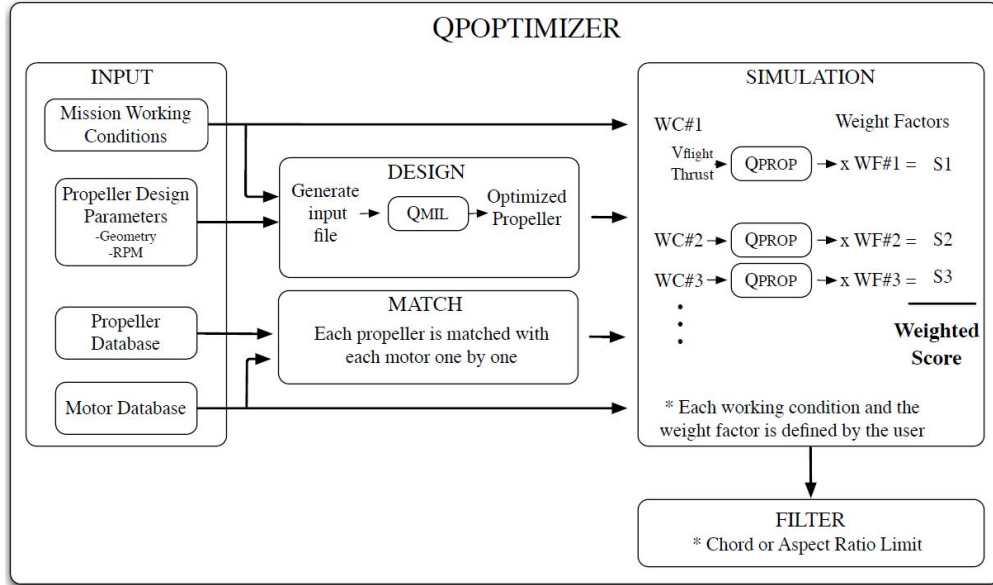


Fig. 3 Main Flow chart of QOPTIMIZER program [12]

5. Optimization Algorithm

Among current multi-disciplinary optimization researches, OpenMDAO is typically used to formulate problem and manage data exchange [5]. It is an open source, high performance platform that manages model hierarchy and assembles optimisation problems. It interacts with the Scipy optimisation module which provides the optimisation algorithms. For the type of problem presented in this paper, a constrained minimization or maximization of multivariate scalar function, the following optimisation algorithms are available to use:

- 1) Trust-region constrained algorithm (trust-constr) : must provide either Jacobian or Hessian matrix, the other could be approximated using finite differentiation.
- 2) Sequential least squares programming (SLSQP) : uses quadratic programming to determine search direction, supports equality / inequality constraints.
- 3) Constrained optimization by linear approximation (COBYLA) : solving approximated linear programming problems, no gradient required, only supports inequality constraints.
- 4) Genetic algorithm : gradient free method, supports both equality and inequality constraints.

Since the inputs to the optimization are user selected parameters (range, duration etc) of the different flight phases, it is highly likely that equality and inequality constraints are needed. The SLSQP algorithm in OpenMDAO was thus chosen to be an initial driver to construct the optimisation structure. In the future, other optimisation drivers such as genetic algorithm could be used to further study the different methodologies.

II. Development of Optimization Tool and Disciplines

A. Aircraft definition module

The design parameters available for aircraft definition are listed in Table 1.

Symbol	Description	Unit
S	Wing surface area	$[m^2]$
AR	Wing Aspect Ratio	$[-]$
λ	Wing taper ratio	$[-]$
Φ	Wing sweep angle	$[^\circ]$
R_{cruise}	Cruise propeller radius	$[m]$
R_{VTOL}	VTOL propeller radius	$[m]$
β_{cruise}	Cruise propeller pitch	$[^\circ]$
β_{VTOL}	VTOL propeller pitch	$[^\circ]$
E_{bat}	Battery capacity	$[Wh]$

Table 1 Design Parameters

Depending on the selected configuration, the aircraft definition module is set up accordingly with initial default values of component locations and dimensions to build the configuration. The different possible configuration are shown as a reference in Fig. 16. The aircraft definition comprises four sub-dictionaries:

- 1) Lifting surfaces : for each lifting surface only one segment is allowed at the moment and the following properties are specified.
 - location of root section leading edge.
 - span.
 - root chord.
 - tip chord.
 - dihedral angle.
 - sweep angle.
 - airfoil or airfoil sets.
 - spanwise panel number.
- 2) Bodies : the current module allows only streamlined body with cylindrical mid-section.
 - location of centre.
 - length.
 - diameter.
 - material density.
- 3) Payloads : point mass that does not have aerodynamic effect.
 - mass.
 - location of centre of gravity.
 - constant electrical power consumption.
- 4) Propulsion groups : each propulsion group consists a motor, an ESC and a propeller.
 - location of propulsion group (propeller centre).
 - orientation of propeller.
 - flight phase that the propulsion group is used (either VTOL, cruise or both).
 - propeller diameter.
 - propeller pitch and chord laws.
 - propeller airfoil.
 - propeller blade number.
 - brushless motor mass or rating.
 - ESC mass or rating.

The aircraft definition parameters are used by the mass and balance module to determine the center of gravity of the aircraft as well as the mass of all the components of the aircraft.

B. Mass and balance module

From Equation 1, the aircraft mass is decomposed into four terms : 1) structural ; 2) propulsion ; 3) battery and 4) payload. Each defined element allows for mass information definition. These elements are typically treated as point

mass defined by specifying mass and the location of centre of gravity. Depending on application, some of these entries are calculated automatically.

The payload mass is expected to be given by the user, and was fixed to be 2.0kg in the current study.

The structural mass differs between lifting surface and bodies. Mass information of lifting surfaces is implied from its MachUp wing segment specification which contains its span, root chord, tip chord and relative thickness. The wing segment is considered to be a trapezoid plate with the same thickness. A global density is specified for all lifting surfaces. The mass of wing segment i is thus found to be the following.

$$m_{w,i} = \frac{\rho_w}{2} (c_{\text{root},i} + c_{\text{tip},i}) \tau b_i \quad (2)$$

For non-lifting bodies, only cylindrical shell is considered. Each body object is defined by its length L_b , outer radius R_b and thickness τ_b . Density is also allowed to be specified individually, otherwise a default global value is used. The mass of body i is found to be the following.

$$m_{b,i} = \rho_{b,i} \pi R_{b,i} \tau_{b,i} L_{b,i} \quad (3)$$

Propulsion mass contains propeller, ESC and motor mass. Currently, the ESC and motor weight model has been implemented by taking the specifications of 26 off-the-shelf Turnigy models from Hobbyking catalogue. Estimation of motor and ESC mass could be made [13, 14]. A linear regression was performed for ESC mass over the rated constant current with $R^2 = 0.81$. The results are presented in Fig. 4. The coefficient of determination value is not a perfect fit, but without specific information, it significant enough to be used as initial guess for a low fidelity model. Further, the models were compared with the linear model in [13], represented by the orange line in Fig. 4, and is shown in good agreement from the previous study. There is also the option to specify the specific mass of the ESCs if the user has a good idea of the weight of the ESCs needed for the preliminary design of the UAV. In the future this model could be further improved by determining the required current draw of the motor and sizing the ESCs accordingly.

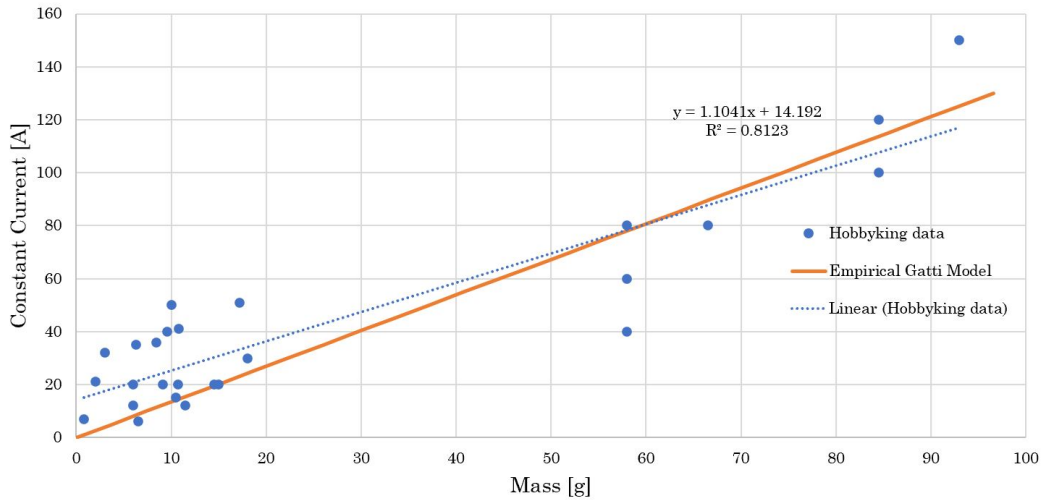


Fig. 4 ESC Constant Current vs Mass Model

The regression model for the motor mass as a function of max current rating could not be validated with reference due to limited data, however for a low fidelity mass model, the obtained power regression shown in Fig 5 was retained. As an alternative, the motor mass could also be estimated using K_V specification, as in [13] shown in Fig. 6. As the case for the ESCs if a specific motor model is known, its mass can be set as constant in the optimisation. Similarly to further improve the fidelity of the motor mass model, the max current rating can be directly driven from the motor requirements derived from the aerodynamic module.

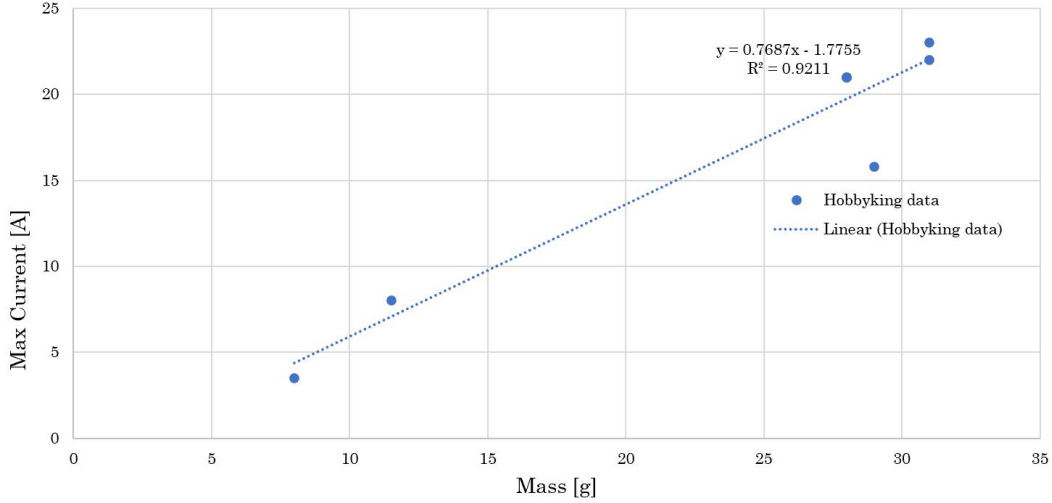


Fig. 5 Motor Max Current vs Mass Model

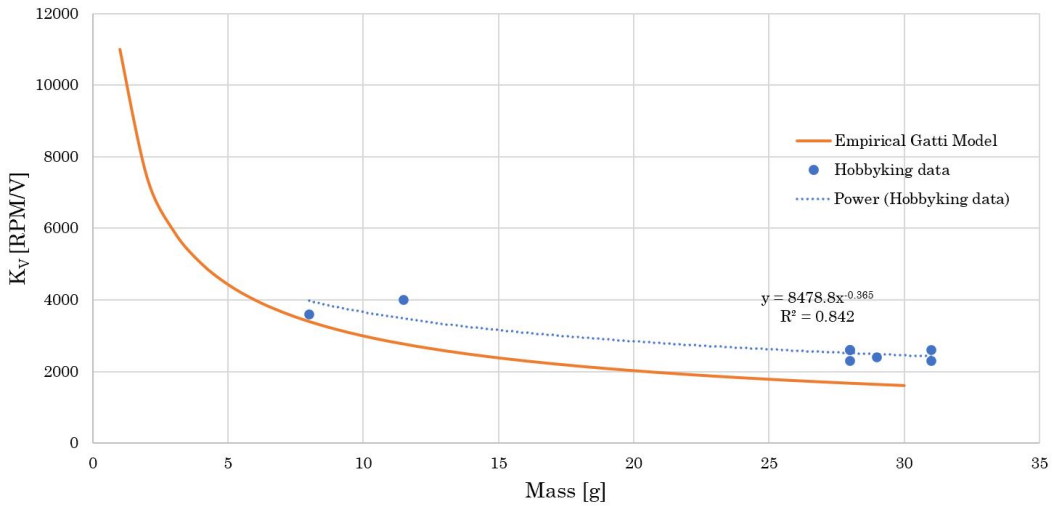


Fig. 6 Motor Kv Rating vs Mass Model

Propeller mass is estimated using empirical formula derived from available commercial catalogue of Aeronaut propellers [15]. For each propeller i ,

$$m_{prop,i} = 1.135B_i R_i^3 + m_{hub} \quad (4)$$

where B_i is number of blades and $m_{hub} = 0.0283kg$.

The battery mass is estimated using specific energy assumption of $k_{bat} = 170Wh/kg$. In optimization routine, battery capacity E_{bat} is always a design parameter and is updated in each optimisation loop. Thus battery mass can be found after each iteration. The location of battery is specified by the user.

$$m_{bat} = \frac{E_{bat}}{k_{bat}} \quad (5)$$

After each component mass is obtained, the total mass m_{total} is calculated using Eq. 1 and is passed on to the structural module.

C. Structural module

Currently the structural module only concerns the wing spar calculation, which computes maximal bending stress σ_{max} , deflection δ and spar mass m_{spar} . Spar dimension ξ is the design parameter that defines cross-section shape. Two cross-sections are available for the analysis as shown in Fig. 7 : circular shell or I-shaped section. In the case of the circular shell, ξ specifies the outer diameter of the tube while for the I-shaped cross section it corresponds to the beam height. The iteration of the outer dimension ξ acts as a loop to find the optimal size of the spar while minimizing its mass considering the aerodynamic loads on the wing.

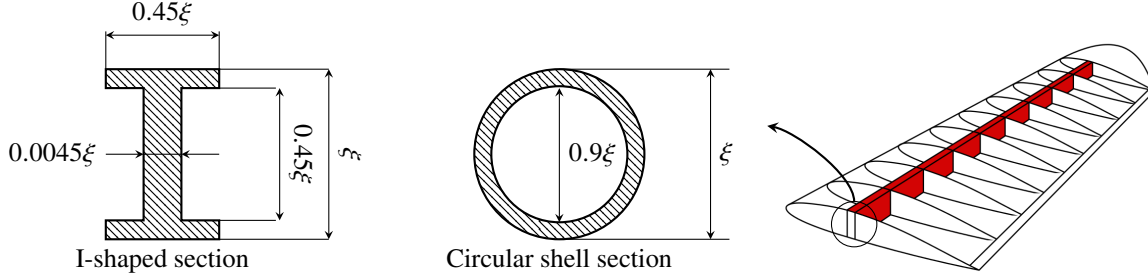


Fig. 7 Wing Spar Cross Sections

As previously introduced the structural model representing the spar is a cantilever beam subjected to elliptical lift distribution. The force F acting on the beam is derived from the total mass m_{total} of the aircraft computed from the mass and balance module while taking into account a maximum load factor of $n_z = 3.5$. For symmetrical flight conditions, we only consider loading over semi-span as shown in Fig. 8.

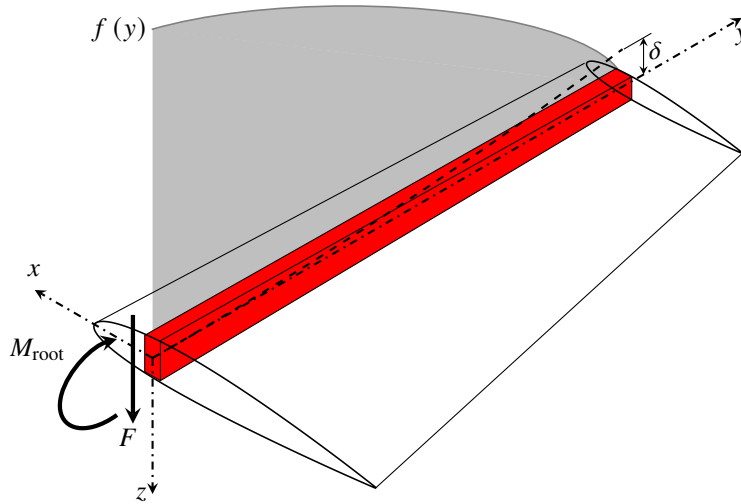


Fig. 8 Wing spar under elliptical load distribution

$$F = \frac{m_{total}}{2} n_z g \quad (6)$$

The moment at the root M_{root} is derived by integrating the elliptical load distribution along the semi-span b .

$$M_{root} = \frac{2Fb}{3\pi} \quad (7)$$

Similarly the maximum deflection at the tip δ_{max} is derived from Equation 7. The centroidal moment of inertia I_c is calculated based on the cross-section of the spar and is the only difference in calculations between the two types of spars.

$$\delta_{max} = \frac{2Fb}{3\pi EI_c} \quad (8)$$

The maximum bending stress σ_{max} in critical section is reached at the upper and lower edges.

$$\sigma_{max} = \frac{M_{root} \xi}{I_c} \frac{\xi}{2} \quad (9)$$

Structural constraints are presented below. The optimizer will solve the problem while observing the following constraints:

- Allowable normal stress: based on the properties of the material of the spar

$$\sigma_{max} \leq \sigma_{allowable} \quad (10)$$

- Tip deflection $\bar{\delta}$: the ratio between the deflection at the tip and the half span b

$$\frac{\delta_{max}}{b/2} = \bar{\delta}_{max} \leq \bar{\delta}_{allowable} \quad (11)$$

- Thickness ratio τ : the ration between the height of the spar and the minimal thickness of the wing

$$\bar{\tau} = \frac{\tau}{\xi} \quad (12)$$

Once the aircraft mass and the mass of the spar have converged, the total mass m_{total} is passed on to the aerodynamic module where it is used as a lift target for trim point calculation.

$$L_{target} = m_{total}g \quad (13)$$

D. Aerodynamic module

A modified version of non-linear lifting line model MachUp [9] was coupled to analyse convertible UAV designs. Non-linear lifting line model has shown great potential in predicting near and post stall behaviour in recent year [16]. Instead of linearised coefficients, these newer methods utilise tabulated 2D airfoil polar. These data can be obtained from either experimental or computational method.

Although detailed implementation of the lifting line model was well documented in [9], a brief introduction of the algorithm and descriptions of the major modifications are presented in this section.

1. Non-linear lifting line model

The MachUp library was developed based on derivation of linear lifting line theory in [17] to calculate lift, drag and moment. The formulation allows multiple lifting surfaces definition. Each lifting surface is made up of several trapezoidal wing segments, which are further discretised to individual panels, as shown in Fig. 9.

At each panel i , a horseshoe vortex system is modelled with constant circulation Γ_i . The bound vortex segment aligns itself with the panel's quarter chord line; semi-infinite trailing vortices stretch downstream in the freestream direction.

The vortex system is solved from Kutta-Jukowsky theory at control point i of each panel, which is designated at the quarter chord position. The boundary condition at control point i is shown in Eq. 14.

$$2 \left| \left(\vec{V}_\infty + \sum_{j=1}^N \vec{v}_{ji} \Gamma_j \right) \times \vec{\zeta}_i \right| \Gamma_i - V_\infty^2 \tilde{C}_{L,i}(\alpha_i, \delta_i) = 0 \quad (14)$$

where $\tilde{C}_{L,i}$ is the sectional lift coefficient as a function of angle of attack α_i and flap deflection δ_i , $\vec{\zeta}_i \equiv \frac{\Delta \vec{l}_i}{\Delta S_i}$ is the ratio between the bound vortex segment vector and the panel surface area.

Further \vec{v}_{ji} is the elementary velocity induced at point i from horseshoe vortex at panel j , as shown in Fig. 10. The elementary induced velocity is calculated from Biot-Savart law in Eq. 15.

$$\vec{v}_{ji} = \begin{cases} \frac{1}{4\pi} \left[\frac{\vec{u}_\infty \times \vec{r}_{j2i}}{r_{j2i}(r_{j2i} - \vec{u}_\infty \cdot \vec{r}_{j2i})} + \frac{(r_{j1i} + \vec{r}_{j1i} \times \vec{r}_{j2i})}{r_{j1i} r_{j2i} (r_{j1i} r_{j2i} + \vec{r}_{j1i} \cdot \vec{r}_{j2i})} - \frac{\vec{u}_\infty \times \vec{r}_{j1i}}{r_{j1i}(r_{j1i} - \vec{u}_\infty \cdot \vec{r}_{j1i})} \right], j \neq i \\ \frac{1}{4\pi} \left[\frac{\vec{u}_\infty \times \vec{r}_{j2i}}{r_{j2i}(r_{j2i} - \vec{u}_\infty \cdot \vec{r}_{j2i})} - \frac{\vec{u}_\infty \times \vec{r}_{j1i}}{r_{j1i}(r_{j1i} - \vec{u}_\infty \cdot \vec{r}_{j1i})} \right], j = i \end{cases} \quad (15)$$

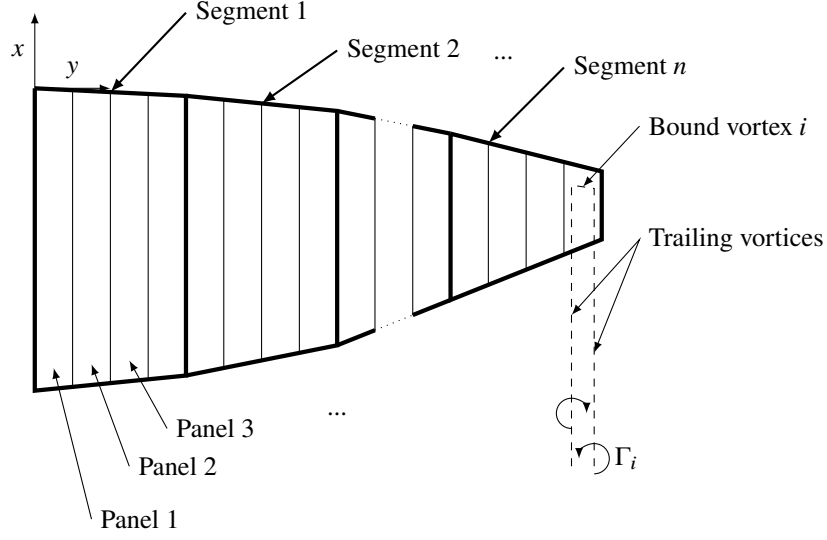


Fig. 9 Lifting surface panels

When $j \neq i$, the elementary velocity consists three terms : the first and third terms are influences from the trailing vortices and the middle term is induced from the bound vortex. When $i = j$, the middle term is zero since the control point lies on the bound vortex.

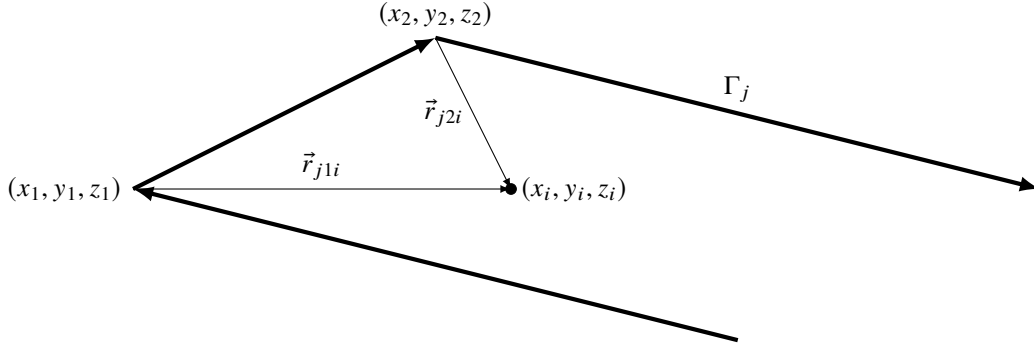


Fig. 10 Horseshoe vortex

Equation 14 can be further simplified by assuming small angle of attack and neglecting higher order terms. These assumptions helped with rapid calculation and robust convergence. A linear system of the bound circulation is derived in Eq. 16.

$$2|\vec{V}_\infty \times \vec{\zeta}_i|\Gamma_i - V_\infty \tilde{C}_{L,i,\alpha} \sum_{j=1}^N \vec{v}_{ji} \cdot \vec{u}_{ni} \Gamma_j = V_\infty^2 \tilde{C}_{L,i,\alpha} (\vec{u}_\infty \cdot \vec{u}_{ni} - \alpha_{0i} + \epsilon_i \delta_i) \quad (16)$$

where $\tilde{C}_{L,\alpha,i}$ is the sectional lift line slope of airfoil at panel i , \vec{u}_∞ and \vec{u}_n is the unit vector in freestream and normal direction, α_{0i} is zero-lift angle of attack at panel i and ϵ is flap efficiency.

However, for the flight conditions encountered by VTOL aircraft, elevated angle of attack is expected. Therefore a modification has to be made to use the non-linear implementation of lifting line model in Eq. 14. The modification was necessary to overcome small angle assumptions associated with the original linear version.

The non-linear lifting line model was implemented with Newton-Raphson iteration. The solution time depends heavily on initial solution, but still fast enough for preliminary design purposes. However a relaxation factor is necessary to ensure convergence. Most successful results were obtained for relaxation factor around 0.8, but divergence can still occur in near-stall and stall condition.

Furthermore, to truly overcome the small angle of attack assumption, airfoil characteristics at high angle of attack

must be taken into consideration. These data are usually obtained from wind tunnel test as numerical solutions for separated flow involves expensive methods such as detached eddy simulation (DES) or large eddy simulation (LES), and thus the data aren't easily available except for a selected studied airfoils [18]. For these airfoils, an option was created to allow reading tabulated data to interpolate lift, drag and moment coefficients according to effective angle of attack and sectional Reynolds number. The other option is to use empirical formulae such as in [19] or [20], which is rather practical as post-stall airfoil characteristics are less dependant on airfoil geometry.

With the aerodynamic model capable to calculate high angle of attack condition, two further modifications were made to correctly present boundary condition for resolving sectional aerodynamic load. These modifications are presented in the following sections.

2. Blade element momentum model and high incidence correction

MachUp library allows for propeller modelling by including a blade element momentum method[9]. Under the model assumptions, each propeller is discretized in radial direction in to n blade elements. At each blade section, its sectional load can be found by applying 2D aerodynamics.

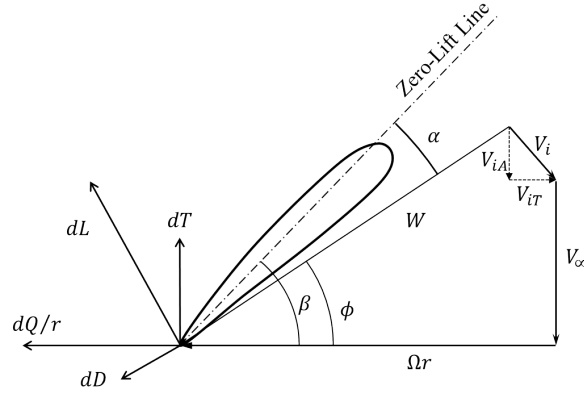


Fig. 11 Flow directions of advancing and retreating blade sections

In Fig. 11, the angle of attack α is calculated as the angle between the total wind velocity W and zero-lift line of the airfoil section. The total wind velocity consists three components : 1. rotation speed Ωr ; 2. freestream V_∞ and 3. induced velocity V_i . The induced velocity is computed iteratively by solving momentum balance in the propeller wake[21].

From the propeller disk plane, one measures the angle ϕ to the total wind velocity and β to airfoil zero-lift line. Therefore, $\alpha = \beta - \phi$. The propeller thrust and power can then be calculated from the integral of the lift and drag coefficient at each blade section.

$$\begin{aligned}
 C_T &= \frac{T}{\rho (\Omega R)^2 S_p} = \int_{\bar{r}_0}^1 \left[\frac{W(\bar{r})}{\Omega R} \right]^2 \sigma(\bar{r}) [C_L(\bar{r}) \cos \phi(\bar{r}) - C_D(\bar{r}) \sin \phi(\bar{r})] d\bar{r} \\
 C_P &= \frac{Q\Omega}{\rho (\Omega R)^3 S_p} = \int_{\bar{r}_0}^1 \left[\frac{W(\bar{r})}{\Omega R} \right]^2 \sigma(\bar{r}) [C_L(\bar{r}) \sin \phi(\bar{r}) + C_D(\bar{r}) \cos \phi(\bar{r})] \bar{r} d\bar{r}
 \end{aligned} \tag{17}$$

However, blade element momentum method is strictly rigorous in axial condition. For convertible aircraft such as quadcopter in forward flight, propeller incidence angle α_p could range between 0 and 90 degrees. The calculated propeller loads thus need correcting. A blade element based approach was developed[22] and incorporated into the MachUp library.

Upon definition, an initial calculation is performed in axial condition with varied tip speed ratio $\lambda = V_\infty/\Omega R$ to obtain zero-incidence thrust and power curves $C_{T_0}(\lambda)$ and $C_{P_0}(\lambda)$.

During analysis, the approach takes into consideration of blade geometry, propeller incidence angle α_p , forward tip-speed ratio μ and axial tip-speed ratio λ_c to compute four propeller loads : thrust coefficient C_T , power coefficient C_P , normal force coefficient C_N and in-plane moment coefficient C_n using the following model. For detailed explanation, interested readers are kindly referred to the work from Leng, et al.[22]

$$C_T(\mu, \lambda_c) = C_T(0, \lambda_c) \eta_T, \quad \eta_T = 1 + \frac{(\mu/\bar{r}')^2}{2(1 - \lambda_c/\lambda_{\infty 0T})} \quad (18)$$

$$C_P(\mu, \lambda_c) = C_P(0, \lambda_c) \eta_P, \quad \eta_P = 1 + \frac{(\mu/\bar{r}')^2}{2(1 - \lambda_c/\lambda_{\infty 0P})} \quad (19)$$

$$C_N(\mu, \lambda_c) = \frac{2\lambda_{\infty 0P} - \lambda_{\infty} \cos \alpha_p}{2\lambda_{\infty 0P} - \lambda_{\infty}} \sin \alpha_p \left. \frac{\partial C_N}{\partial \alpha_p} \right|_{\alpha_p=0, \lambda_{\infty}}, \quad \left. \frac{\partial C_N}{\partial \alpha_p} \right|_{\alpha_p=0} = \frac{1}{2\pi^2} \frac{k_s f(\lambda_i) \sigma I_1}{\frac{I_1}{I_1 - \Delta} + k_a \sigma I_1} \quad (20)$$

$$C_n(\mu, \lambda_c) = \frac{2\lambda_{\infty 0T} - \lambda_{\infty} \cos \alpha_p}{2\lambda_{\infty 0T} - \lambda_{\infty}} \sin \alpha_p \left. \frac{\partial C_n}{\partial \alpha_p} \right|_{\alpha_p=0, \lambda_{\infty}}, \quad \left. \frac{\partial C_n}{\partial \alpha_p} \right|_{\alpha_p=0} = \frac{1}{\pi^2} \frac{k_s f(\lambda_i) m}{1 + k_a \sigma (I_1 - \Delta)} \quad (21)$$

3. Wake deformation model

Original propeller wake was extended downstream along rotation axis as a straight cylinder. The wake model was then used to calculate immersed wing control points where propeller induced velocity needed to be included in lifting line model. Therefore, the accuracy of lifting line calculation depends on correct wake position.

The earlier model however fails to take freestream convection into consideration. In reality, as forward flight speed increases, the wake streamtube will be "skewed" or displaced in direction perpendicular to rotation axis. This phenomenon is illustrated in Fig. 12, as tip blade vortices of a forward flying helicopter were visualised by background-oriented schlieren (BOS) method [23].

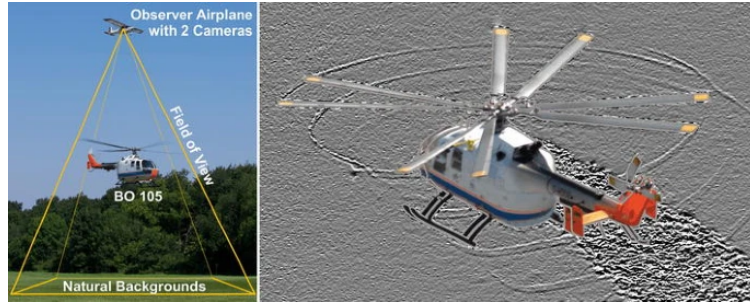


Fig. 12 Blad tip vortices visualised from background-oriented schlieren (BOS) method [23]

The angle between ultimate slipstream axis and the rotational axis is referred to as wake skew angle χ . χ can be accurately estimated from momentum theory [21, 24].

In Fig. 13, a side-view illustration of the wake displacement is presented.

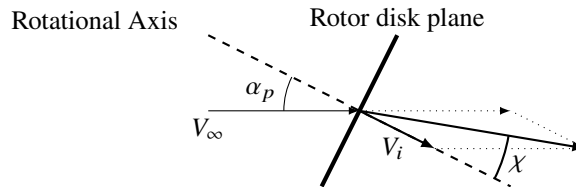


Fig. 13 Wake Skew Angle

Downstream of the propeller disk, the flow component constitutes two components :

- 1) Freestream V_{∞}
- 2) Induced velocity V_i

V_i is supposed to be aligned with rotation axis since the normal force on disk plane is usually one order of magnitude smaller than thrust. The skew angle χ is thus originated from the freestream component perpendicular to rotation axis. Thus the ultimate wake skew angle is found

$$\chi = \arctan \frac{V_\infty \sin \alpha_p}{V_\infty \cos \alpha_p + V_i}$$

The wake skew angle is assumed to be established immediately downstream disk plane, and its direction \hat{i}_w is used to determine wing immersed points, where for a given point A

$$|\vec{r}_{w,A}| = |(\vec{r}_A - \vec{r}_{O_p}) \times \hat{i}_w| \leq R_p$$

where O_p is the center of propeller, R_p is propeller radius and \vec{r} is the position vector to respective point.

4. Interaction with optimisation algorithm

The aerodynamic module takes the aircraft configuration and given mission profile as inputs. The geometric specifications are compiled into .json file which MachUp has access to. If the aircraft configurations has a different propulsive groups for cruise and VTOL configurations, it is possible to have two .json files as geometry input for each configuration. For example in the quadplane configuration, the VTOL version (Figure 14a) contains lifting propellers used during VTOL phase and any relevant lifting surfaces while other propulsion groups or lifting surfaces were ignored in the aerodynamic model (but their mass impact is kept). According to [19], a slender wing at 90° angle of attack generates drag coefficients between 0.7 to 1.0. At extreme climb speed of $3m/s$ for a long endurance aircraft, this usually constitutes 5% of aircraft total gravity, and thus is ignored in the current study.

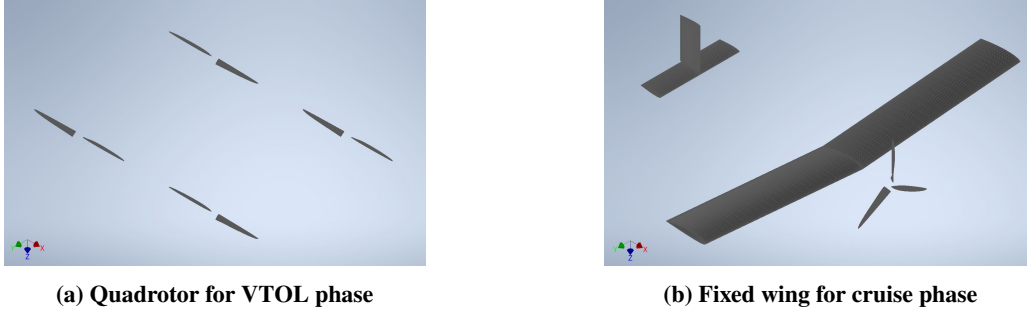


Fig. 14 Quadplane Machup model for VTOL and cruise phase calculation

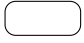

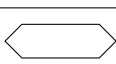
Similarly the cruise configuration (Figure 14b) eliminates any propulsion groups or lifting surfaces to be ignored in cruise analysis. The mass and balance module generates desired lift and moment for equilibrium flight.

For each flight segments defined in mission profile, the aerodynamic module performs a separate calculation. The aircraft configuration (either VTOL or cruise) must be specified for each phase, to determine the respective geometry input. Flight condition is also provided from the flight segment definition.

MachUp trim analysis based on L_{target} is then executed based on the flight phase to obtain aircraft state and control surface state. These are then fed back to MachUp force analysis to obtain aircraft force and moment information, as well as propeller shaft power P_{shaft} which is fed into the performance module detailed in the following section.

E. Flight phase analysis

For a given candidate configuration, the performance and structural parameters are analysed and computed for each designated flight condition. These calculates results from the coupling between the aforementioned three modules : mass and balance, structure and aerodynamics. The aerodynamics discipline yields performance in flight, while the weight discipline will estimate required initial structural mass and will iterate within the structural discipline to size the spar according to the constraints and finally update the total mass. The aerodynamics optimization will revolve around finding the best wing planform for the mission profile.

Legend	Symbol
Optimiser	
OpenMDAO Components	
Calculation Module	

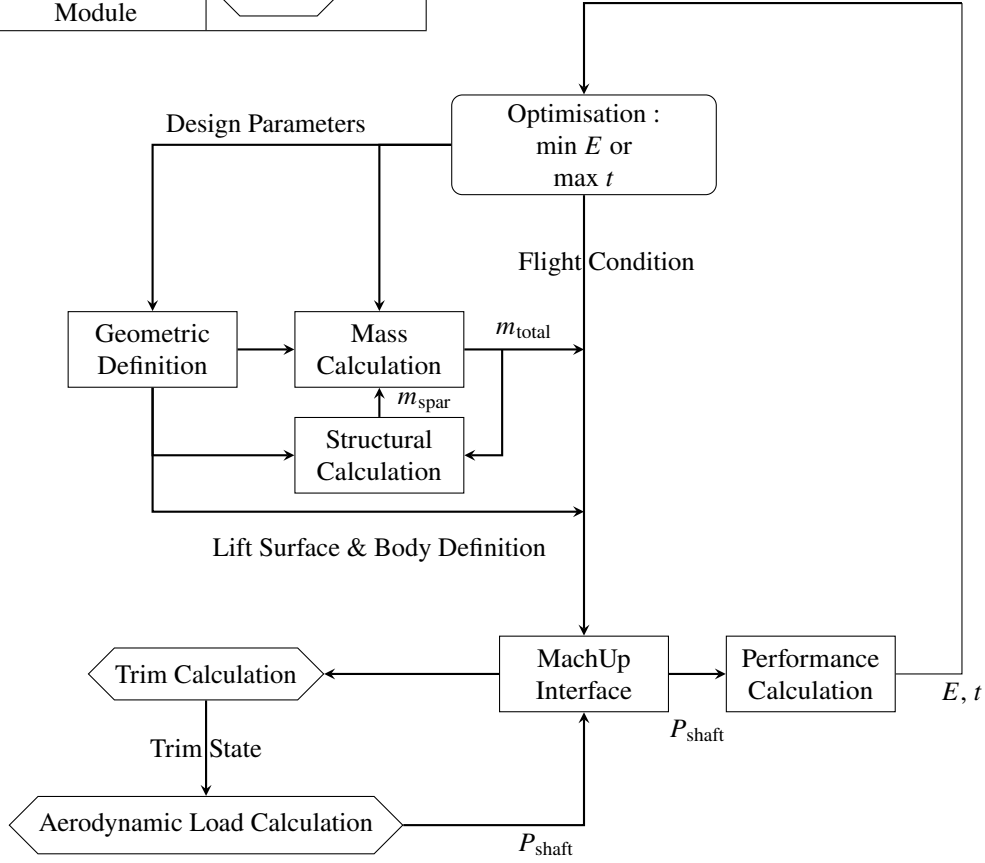


Fig. 15 Design Flow Chart for a Single Flight Phase

Figure 15 outlines the data flow in the optimisation algorithm for a single flight phase. At the top is the optimisation component which manages the iteration loop by evaluating cost function and changing design parameters accordingly using the SLSQP algorithm. For current study, only mission energy E and endurance t_E are considered as cost function.

The respective design parameters are propagated into geometry and mass calculation modules. The geometry module takes the geometric design parameters and completes the aircraft definition with further assumptions, which are to be introduced for specific aircraft configurations.

The performance calculation takes input from the results from MachUp calculations and propulsion group definition to assess the flight performance.

For all N flight segments, only one segment n is allowed to have unspecified flight time, and in this case the algorithm maximises flight endurance of flight phase n .

Shaft power for each flight segment is provided from aerodynamic module for each propulsion group. The performance module then calculates total electric power consumption from Eq. 22.

$$P_{elec} = \frac{P_{shaft}}{\eta_m \eta_{ESC}} = \frac{P_{shaft}}{\eta_{elec}} \quad (22)$$

where η_{elec} is the electrical efficiency in the propulsion group.

The total power consumption is the sum of consumption from each propulsion group i and an additional constant avionic consumption, which is set to zero for the current study in order to highlight aerodynamic aspects.

$$P_{\text{total}} = \sum_{i=1}^N P_{\text{elec},i} + P_{\text{misc}} \quad (23)$$

Once total power consumption is known for each flight segment j , the remaining flight time for segment m is trivial to find.

$$t_n = \frac{\eta_{\text{bat}} E_{\text{bat}} - \sum_{j=1, j \neq n}^N P_{\text{total},j} t_j}{P_{\text{total},n}} \quad (24)$$

and is passed on as cost function.

The total endurance could then be found to be

$$t_E = \sum_{j=1}^N t_j \quad (25)$$

In the case that flight time and velocity are specified for all flight segments, the algorithm will try to minimise full mission energy consumption as can be found in Eq. 26.

$$E_{\text{total}} = \sum_{j=1}^N P_{\text{total},j} t_j \quad (26)$$

III. Optimization Problem

A. Problem Setup

The problem definition is done using the methods and structure available from OpenMDAO. The *Problem* class is used to define the top level container holding all the other objects. It contains all the system and its subsystems that build the model hierarchy. The *Component* class represents the lowest-level functionality and performs the mapping between input and output values which can be based on basic calculations or more complex functions. The *Group* class contains components or other groups or a combination of both. The main purpose of groups is to manage the data dependency between the subsystems but also to package components together that fall under the same discipline.

There are two major ways to analyze the mission, the optimization can be done for a single flight phase or for a combination of flight phases. For the latter method, there are two options available: minimize the overall mission energy consumption or maximize the endurance of a single phase based on the analysis of the other phases. The distinction between a single phase or several phases is done using the *flight_phase* variable. While the distinction between minimizing energy and maximizing endurance is done with the flight phase definition dictionary and is further explained in the following section.

During the initial development, the focus was on setting up the problem to optimize the UAV for a single flight phase as per Figure 15. Once the single phase optimization was validated, the overall flight phase optimization was developed with every flight phase now becoming a component of the problem. The sub-structure of each of the flight phases was maintained, so that the aerodynamics, structural integrity and mass estimation are calculated for each of the flight phases. Since the flight phases are connected with the same design variables we obtain a coupled model that needs to be converged in order for the outputs to be valid. This circular dependency between the phases requires a non-linear solver so that they can be converged by iterations. The chosen non-linear solver is the Newton solver. It is well suited for closely coupled problems. [5]. In the context of OpenMDAO, this type of problem is called a multidisciplinary analysis (MDA), which is an iterative process that will compute a set of coupling variables that will satisfy the consistency constraints between the coupled model, in this case the coupled flight phases.[25]

1. Flight Phases, Configuration and Independent Variables Definition

The flight mission is split up into several flight phases defined by the user in the *flight_phases* dictionary, such as : VTOL, climb, cruise, loiter, descent and landing. Each flight phase has the following keys: name, nature, elevation, V_x , V_z and duration. The duration is particularly important since it governs the setup of the problem: all flight phase duration can be defined or a single flight phase can have its duration set to zero. The first option sets the optimisation objective to be the minimisation of overall mission energy consumption while the second option sets it to the maximisation of a particular flight phase endurance. The speeds specified are in terms of calibrated airspeed $V_{CAS} = V_\infty \sqrt{\rho_\infty / \rho_0}$, where ρ_0 is air density in standard sea level condition. The flight phases are categorised into two families: *VTOL* nature and *cruise* nature. This defines the aircraft configuration as seen by the aerodynamic module in the particular flight phase.

The incorporated MachUp library allows for various combinations of lifting surfaces and propulsion systems representative to convertible UAVs, and the current study concentrates on three types of UAV configurations: quadcopter, quadplane and tilt-rotor when performing the optimization. The different configuration baselines are set up using a .json file and can be modified to meet specific requirements or geometries.

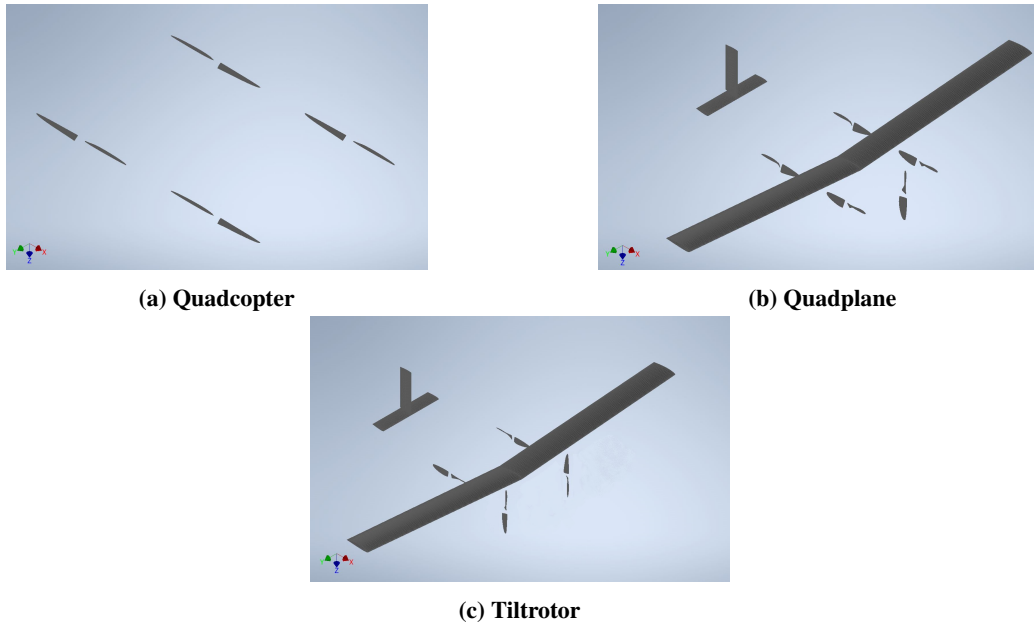


Fig. 16 Studied VTOL aircraft configurations

- 1) Quadcopter (Fig. 16a): The rotor aircraft employs four lifting propellers having elliptical chord and ideal pitch distribution, defined by the radius R_{VTOL} and pitch angle β_{VTOL} at $75\%R_{VTOL}$. An X-shaped fuselage frame is calculated linking all four propellers with payload mass situated in the centre. No wing surface or structure is equipped for this configuration.
- 2) Quadplane (Fig. 16b): This is a combination of quadcopter and a traditional aircraft. It has four lifting propellers and a cruise propeller which is defined independently by R_{cruise} and β_{cruise} . The lifting propellers are only used in VTOL configuration and cruise propeller operates only in cruise configuration. The aircraft has a main wing in the middle of front and rear lifting propeller pairs, its planform shape subjects to the definition of design parameters. A main spar is considered to support the lift load in cruise configuration. A tail section is sized with horizontal tail volume coefficient $V_H = 0.45$ and vertical tail volume coefficient $V_V = 0.02$. The aircraft has three extra streamlined bodies : fuselage between cruise propeller and horizontal tail ; two booms connecting each front and rear propeller through the wing.
- 3) Tiltrotor (Fig. 16c): This configuration is similar to quadplane definition without the cruise propulsion group. The front propeller pairs operate in both VTOL and cruise configurations but it rotates from upward facing orientation in VTOL configuration to forward facing in cruise configuration. It is possible to use different propeller geometries for front and rear propeller pairs, however it is rarely seen in practical design due to spar part requirements from frequent propeller damages.

There are several variables that need to be defined for the optimization and are grouped as follows: wing structure, flight condition, propulsion group parameters and are specified in Table. 2.

Group	Variable	Value	Unit	Comment
Wing structure	$\bar{\delta}$	0.05	-	Tip deflection
	E	150	GPa	Spar Young's modulus
	$\sigma_{\text{allowable}}$	3	GPa	Yield stress
	ρ_{spar}	1600	$kg \cdot m^{-3}$	Material density
	n_z	3.5	-	Maximal normal load factor
	Beam Type	2	-	1 for I-shaped section ; 2 for circular shell section
Flight condition	ρ_{air}	1.225	$kg \cdot m^{-3}$	Air density
	ν_{air}	1.5×10^{-5}	$m^2 \cdot s^{-1}$	Air kinematic viscosity
	g	9.81	$m \cdot s^{-2}$	Gravitational acceleration
Propulsion group	η_{elec}	0.75	-	Electrical efficiency
	η_{bat}	0.90	-	Usable battery capacity
	k_{bat}	170	$Wh \cdot kg^{-1}$	Battery specific energy

Table 2 Independent Variables

2. Design Variables

The previously described design variables for the different disciplines can be enabled or disabled in the current problem definition. This is done using the *add_design_var* method of the OpenMDAO library. Global design variables are applicable to all types of phases analyzed while local design variables are only applicable to one type of flight phase. The design variables along with their upper and lower bounds are listed in the table below:

Variable	Min	Max	Unit	Applicability
AR	8	15	-	All
S	0.2	2.0	m^2	All
E_{bat}	500	1000	Wh	All
R_{VTOL}	0.15	0.45	m	VTOL or All
β_{VTOL}	5	45	$^\circ$	VTOL or All
R_{cruise}	0.15	0.45	m	Cruise
β_{cruise}	5	45	$^\circ$	Cruise
λ	0.1	1.0	-	Cruise
ϕ	0	45	$^\circ$	Cruise
ξ	0.005	0.05	m	Cruise

Table 3 Design Parameters

Notice that the VTOL propellers could also be designated for cruise configuration, this is to accommodate configurations that do not have an independent propulsive group for cruise flight, such as quadcopter or some tiltrotor aircraft.

3. Constraints

The SLSQP driver allows the definition of inequality constraints using the *add_constraint* method. The constraints and their lower bound and upper bound are listed in Table 4. The mean geometric chord c and wing span b constraints have been selected to match the design space of current existing commercial convertible UAVs. The battery capacity constraint ensure a reserve battery capacity of 10% following the design flight mission completion. The limit stress $\sigma_{\text{allowable}}$ value is representative of the yield strength of commercial carbon fiber reinforced polymer. The wing tip deflection ratio $\bar{\delta}$ is set at 5% of the half span of the wing based on engineering intuition. The thickness ratio $\bar{\tau}$ was chosen to be 10% meaning that the spar must not occupy more than 90% of the wing thickness.

Variable	Min	Max	Unit
c	0.05	0.30	m
b	0.00	3.50	m
E_{total}	-	$\eta_{\text{bat}} E_{\text{bat}}$	Wh
t_n	0	-	min
$C_{L_{\text{max}}}$	-	1.20	-
σ_{max}	-	3×10^9	Pa
$\bar{\delta}_{\text{max}}$	-	0.05	-
$\bar{\tau}$	1.10	-	-

Table 4 Constraints

4. Objective

As previously stated, there are two possible objectives depending on the definition of flight phases. If all flight phases are defined with non-zero flight duration, the objective is to minimise total energy consumption from all N flight phases.

$$\min (E_{\text{total}}) = \min \left(\sum_{j=1}^N P_{\text{total},j} t_j \right) \quad (27)$$

If one particular flight phase n has flight duration defined as zero, the objective is to maximise duration in of flight phase n , hence the flight endurance.

$$\max (t_n) = \max \frac{\eta_{\text{bat}} E_{\text{bat}} - \sum_{j=1, j \neq n}^N P_{\text{total},j} t_j}{P_{\text{total},n}} \quad (28)$$

5. XDMSM diagram

The eXtended Design Structure Matrix (XDMSM) is a tool used to visualize MDO processes [25]. It permits the visualisation of the optimization problem by representing the components, variable connections and optimization algorithms. The order in which the algorithm runs is also represented with a numbering system and lines. The XDMSM is therefore a convenient way of illustrating all the data and process flow of the optimization problem. Green boxes represent generic processes, while parallelograms are used for data input and output. Components that refer to an iterative procedure are represented using rounded rectangles: purple rounded boxes represent the main driver which in this case is the SLSQP driver and the orange rounded boxes represent the non-linear solver, here the Newton solver. The circular dependency between components is illustrated with solid grey lines connecting the green boxes as shown in Figure 17. Table 5 defines the mathematical notations used in figure 17.

Symbol	Definition	Composition
x	Vector of global design variables	$(AR, S, E_{bat}, R_{cruise}, \beta_{cruise}, R_{VTOL}, \beta_{VTOL}, \lambda, \phi, \xi)$
x_{VTOL}	Vector of VTOL design variables	$(AR, S, E_{bat}, R_{cruise}, \beta_{cruise}, R_{VTOL}, \beta_{VTOL})$
x_{Cruise}	Vector of Cruise design variables	$(AR, S, E_{bat}, R_{cruise}, \beta_{cruise}, \lambda, \phi, \xi)$
cst	Vector of constraints	$(c, b, E_{total} \text{ or } t_n, C_{Lmax}, \sigma_{allowable}, \bar{\delta}, \bar{\tau})$
$()^*$	Vectors or variables at their optimal value	N/A
$()^0$	Initial value of vectors or variables	N/A

Table 5 Mathematical notation for MDO problem data

For the current optimization problem of maximizing the endurance of a single phase, a multidisciplinary feasible architecture (MDF) [26] was selected. The multidisciplinary design feasible architecture can be seen as a conversion from a single discipline case to multiple discipline case where the single discipline is replaced by the MDA. Here the previously introduced flow chart (Figure 15) becomes a single component representing each of the flight phases. The sequence of operations is shown by the black line and follows the numbering system. The MDF architecture for the current problem is presented below:

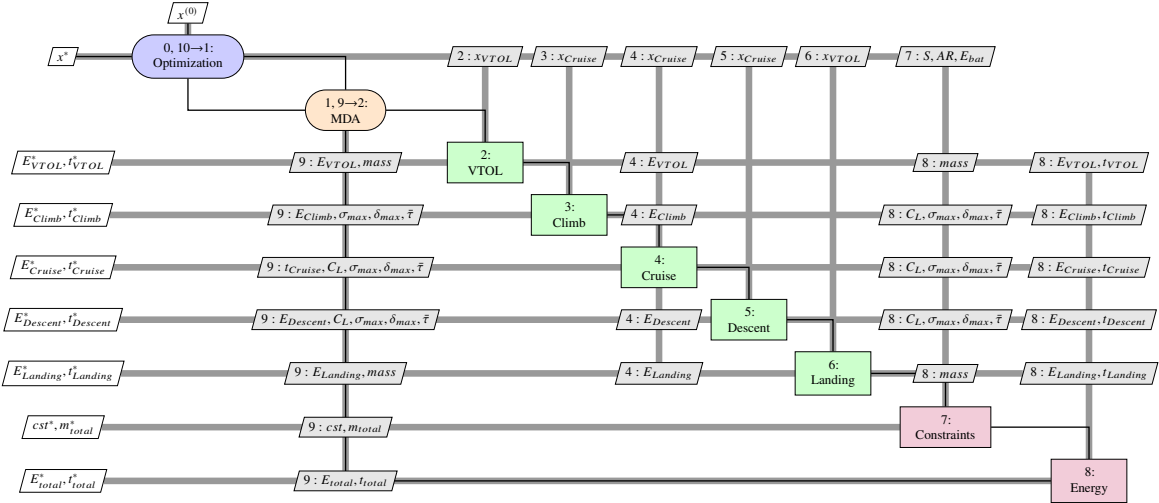


Fig. 17 Maximize single phase endurance XDSM

The sequence of operations in the current problem is as follows:

- 0) Pass initial data (design variables) to Optimization and MDA drivers.
- 1) Initiate MDA using Newton solver.
- 2) Evaluate VTOL phase and return energy consumed and endurance.
- 3) Evaluate climb phase and return energy consumed and endurance.
- 4) Evaluate cruise phase using energy from other phases and determine remaining energy and endurance.
- 5) Evaluate descent phase and return energy consumed and endurance.
- 6) Evaluate landing phase and return energy consumed and endurance.
- 7) Compute constraint function values.
- 8) Compute cost function values.
- 9) Check MDA convergence. If it has not converged, return to 2; otherwise, continue.
- 10) Compute new design point. If optimization has not converged, return to 1; otherwise, return optimal solution.

The architecture above is maintained for both scenarios presented in the following section with the exception of the different flight phases based on the scenarios.

B. Test Cases Setup

The optimization algorithm is first tested on a baseline mission profile comprising vertical take-off, climb, cruise, descent and vertical landing as shown in Table. 6, with 60 minutes total endurance. Tiltrotor configuration is considered to allow comparison with Tron F90+[27], a similar vehicle from Quantum System. An additional 80W electrical power consumption was considered to better simulate the operational condition.

Parameters	TO	Climb	Cruise	Descent	Landing
Initial Elevation [m]	0	60	600	600	60
V_z [m/s]	2.0	1.5	0.0	-1.0	-1.0
V_x [m/s]	0.0	15.0	18.0	15.0	0.0
Duration [min]	0.5	6.0	43.5	9.0	1.0
Configuration	VTOL	Cruise	Cruise	Cruise	VTOL

Table 6 Baseline mission specifications

Commercial UAVs are optimized for one phase in which they spend the most time based on their application. It is therefore of interest to test scenarios in which the endurance of a single flight is optimized. Two typical scenarios were analyzed, without the previously mentioned 80W miscellaneous electrical power consumption.

1. Scenario 1: maximizing cruise endurance

In this scenario, the UAV is expected to perform a vertical take-off up to 60m, then to follow a 10% climb gradient at 15m/s no-wind ground speed up to 600m. The aircraft cruise at 18m/s for a maximal allowable time until its battery capacity reaches the final reserve level plus energy for a 6.7% descent to 60m followed by a vertical landing. This scenario is typical for long range surveillance mission or autonomous delivery flights. The goal is to choose the optimal design parameters to maximise the cruise endurance.

A detailed specification is provided in Table. 7.

Parameters	TO	Climb	Cruise	Descent	Landing
Initial Elevation [m]	0	60	600	600	60
V_z [m/s]	2.0	1.5	0.0	-1.0	-1.0
V_x [m/s]	0.0	15.0	18.0	15.0	0.0
Duration [min]	0.5	6.0	-	9.0	1.0
Configuration	VTOL	Cruise	Cruise	Cruise	VTOL

Table 7 Scenario 1 mission specifications

For quadcopter, the aircraft configuration won't change between flight phases, while for quadplane and tilt-rotor, only take-off and landing will be analysed using VTOL configuration.

2. Scenario 2: maximizing loiter endurance

The second scenario consists largely of the same flight phases as previous scenario, except that the cruise endurance is fixed at 70.3 minutes and an additional VTOL loiter phase is added. This scenario corresponds to local surveillance mission at remote site. The mission specification represents an action radius of 45km from the base and the surveillance site. The goal is thus to optimise the aircraft configuration to achieve maximal on-site loiter time.

The mission specification is detailed in Table. 8.

Parameters	TO	Climb	Cruise	Loiter	Descent	Landing
Initial Elevation [m]	0	60	600	600	600	60
V_z [m/s]	2.0	1.5	0.0	0.0	-1.0	-1.0
V_x [m/s]	0.0	15.0	18.0	0.0	15.0	0.0
Duration [min]	0.5	6.0	70.3	-	9.0	1.0
Configuration	VTOL	Cruise	Cruise	VTOL	Cruise	VTOL

Table 8 Scenario 2 mission specifications

C. Results and discussions

1. Baseline Mission Profile

The design parameters optimised for baseline mission profile are presented in Table. 9. Available data from Tron F90+ tiltrotor is displayed to allow comparison with an operational vehicle.

	Baseline Optimization	Tron F90+
AR [-]	14.2	13.7
S [m^2]	0.865	0.892
Span [m]	3.5	3.5
Taper Ratio [-]	0.942	Elliptical
R_{VTOL} [m]	0.2011	-
β_{VTOL} [$^\circ$]	24.5	-
Battery Capacity [Wh]	1000	-
Mass [kg]	14.0	13.5
Cruise L/D [-]	14.1	-
Total Endurance [min]	60.0	60.0

Table 9 Design parameters optimized for baseline mission and Tron F90+ specifications [27]

At conceptual design stage, the optimized vehicle dimensions resemble closely to those of the production aircraft. The wing surface area and total mass are within 5% of the published specification, with the Tron F90+ having a lower wing loading. It is therefore promising that the tool is capable to simulator typical convertible mission and generate accurate initial size for conceptual design considerations.

2. Scenario 1

Design parameters optimised for each configuration are presented in Table. 10.

	Quadcopter	Quadplane	Tilt-rotor
AR [-]	-	14.1	14.6
S [m^2]	-	0.866	0.839
Taper Ratio [-]	-	0.96	1.00
R_{VTOL} [m]	0.4500	0.2044	0.1988
β_{VTOL} [$^\circ$]	6.0	8.6	29.9
R_{cruise} [m]	-	0.2064	-
β_{cruise} [$^\circ$]	-	17.6	-
Battery Capacity [Wh]	1000	1000	1000
Mass [kg]	12.0	14.7	12.2
Cruise L/D [-]	-	14.0	14.7
Cruise Endurance [min]	36.8	162.0	102.1
Total Endurance [min]	53.3	178.5	118.6
Mission Range [km]	53.2	188.4	123.8

Table 10 Design Parameters for scenario 1

Under scenario 1, the high speed cruise phase takes large part of airborne endurance. The respective aircraft design thus highly favors the parameters that minimise cruise power consumption. For all three configurations, the first priority in attempt to maximise endurance is to increase battery capacity. Within the given constraints, the maximal battery capacity of $1000Wh$ is reached in all three cases.

For quadcopter, both near-hover and cruise phase rely on rotary wing aerodynamics. The aircraft thus features large, fine pitch propellers which create less induced power. The propeller radius of $0.45m$ is similar to the design of helicopter whose propulsion system consists a light loaded main rotor. The maximal endurance reaches 53.3 minutes which is the smallest among the three configurations but a relatively high number among available quadcopters. Also notice that the maximal endurance is less than the 70.8 minutes required cruise endurance in scenario 2, and thus quadcopter configuration won't be considered for scenario 2.

For quadplane, the cruise phase is sustained by wing aerodynamic loads and a dedicated propulsion group. In consequence, a slender straight wing is desired, whose aspect ratio reaches 14.1. It is worth noting that the aspect ratio didn't reach its upper bound of 15. This is constrained by the minimal allowable thickness of airfoil to embed a sufficiently strong structure, where as the aspect ratio increases, the airfoil section dimension diminishes. The cruise propeller has a radius of $0.2064m$ and a higher pitch than VTOL propellers, which is more efficient in high speed cruise. The VTOL propeller size is also much smaller than those of the quadcopter. Since near hover flight only takes 1.5 minutes, or less than 1% of total endurance, it is acceptable to install lighter but less efficient propeller to achieve VTOL capability. Overall, in the given scenario, quadplane configuration is possible to achieve the maximal endurance of 178.5 minutes among three candidates.

The tilt-rotor situates at a middle ground between quadcopter and quadplane. It features a slender wing for cruise flight but don't have a dedicated cruise propulsion group. The wing planform is very similar to the quadplane wing, however the lift to drag ratio increases by 1 due to the beneficial interaction of propeller slipstream. The propeller, or proprotor, installed is a compromise between ideal hover propeller and cruise propeller. Its radius is 56.0% smaller than that of the quadcopter but its pitch increases by almost 24° to provide required thrust in high speed condition. The cruise performance is significantly impacted by the propeller efficiency achieving an endurance 34.2% less than the quadplane endurance.

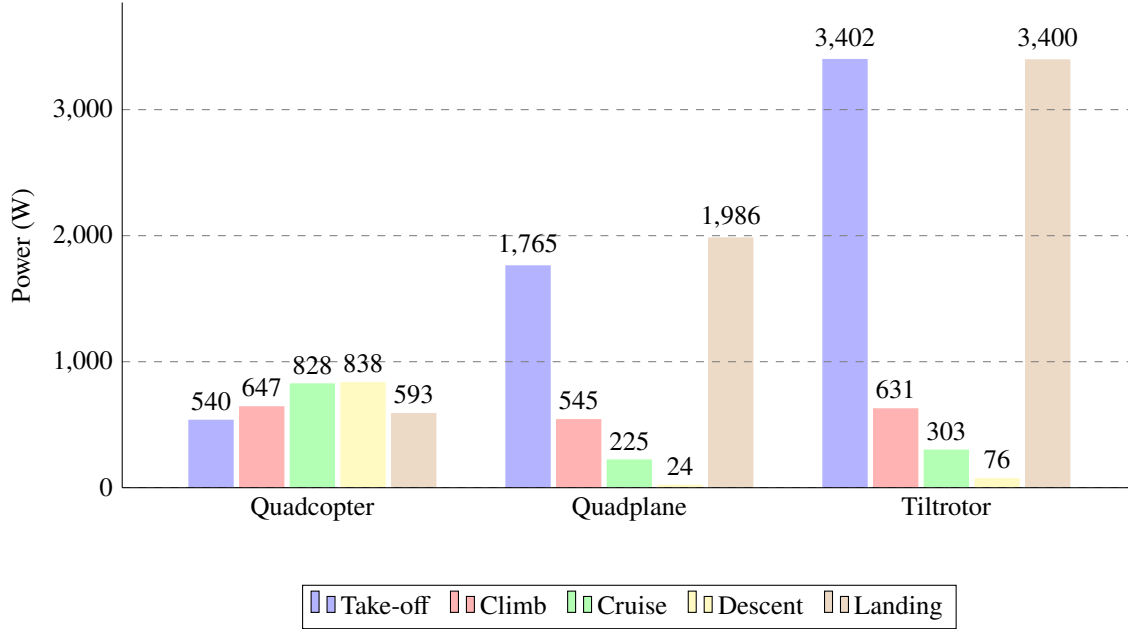


Fig. 18 Power consumption by flight phase in scenario 1

A breakdown of electrical power consumption by flight phase is provided in Fig. 18. The quadcopter configuration shows lowest disparity between flight phases but its cruise power consumption remains the highest both relative to different flight phases and to the other two configurations. The quadplane consumes much higher than the quadcopter in VTOL phase, but only consumes less than a quarter in cruise phase. The tilt-rotor has the highest VTOL power consumption due to its high pitch propeller, while its cruise performance is comparable to a quadplane. Overall, power consumption demonstrates that a compromised system applied to both hover and cruise flight phase may result in lesser performance in either flight phase.

3. Scenario 2

Optimal design parameters to maximise loiter endurance under scenario 2 are shown in Table. 11. Only quadplane and tilt-rotor configurations were analysed as it has been demonstrated clearly in scenario 1 analysis that quadcopter won't have the range capability to satisfy the mission profile

	Quadplane	Tilt-rotor
AR [-]	13.0	14.0
S [m^2]	0.945	0.873
Taper Ratio [-]	1.00	0.93
R_{VTOL} [m]	0.4010	0.2627
β_{VTOL} [°]	7.9	21.0
R_{cruise} [m]	0.2101	-
β_{cruise} [°]	22.8	-
Battery Capacity [Wh]	1000	1000
Mass [kg]	16.0	14.1
Cruise L/D [-]	11.5	14.3
Loiter Endurance [min]	16.1	4.8
Total Endurance [min]	102.9	91.6

Table 11 Design parameters for scenario 2

The two configurations are largely similar to the previous designs but many design choices now favors more towards VTOL performances. For the quadplane, the radius of VTOL propellers doubles that calculated in scenario 1, and is only 10.8% smaller than the quadcopter. This results in an increase in aircraft mass, and in turn, a larger wing and cruise propeller are needed. Combined, the aircraft mass increased by 8.8% to achieve a maximum of 16.1 minutes for loiter.

For the tiltrotor, similar change appeared for its propeller design. Its radius increased from 0.1988m to 0.2627m, a smaller magnitude compared to quadplane to keep its cruise efficiency. Propeller pitch also decreased from 29.9° to 21.0° in favor of loiter phase. The tiltrotor can sustain a 4.8 minutes loiter within a maximal flight time of 91.6 minutes.

The breakdown in power consumption including loiter flight is shown in Figure. 19. Similarly as in Scenario 1, the independent propulsion architecture in quadplane design is able to achieve lower power consumption in all flight phases, and notably a 25% reduction in loiter phase compared to tiltrotor. However, the change in design objective also produced a more balanced tiltrotor design, whose power consumption in VTOL phase reduced generally by 48% thanks to the reduced propeller disk loading.

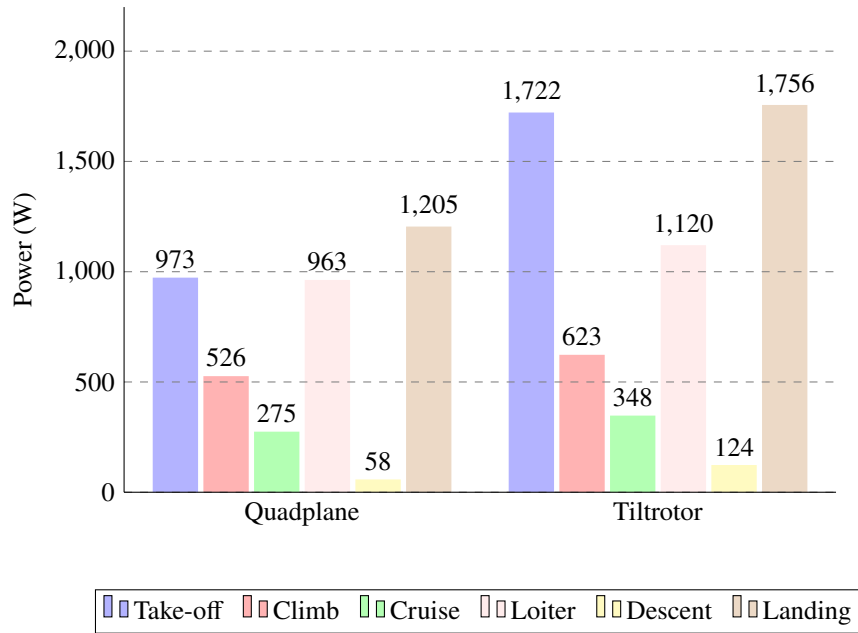


Fig. 19 Power consumption by flight phase in scenario 2

IV. Conclusions and future improvements

This paper proposed a multi-disciplinary optimisation algorithm for preliminary convertible UAV design. The algorithm takes advantage of validated rapid reduced-order methods for propeller and lifting surface aerodynamic analysis. It is thus capable to consider vastly different aircraft configurations for various mission profiles. It has also been shown that other disciplines could be connected as subsystems to include considerations in structure, flight control and electrical systems. Optimum results could be achieved in a relatively fast and robust fashion.

Preliminary design results have been presented over two application scenarios to demonstrate the algorithm's capability in adapting aerodynamic design to specific mission profile. It has been observed that despite the increased aircraft mass by combining fixed-wing and quadcopter configurations, the quadplane's dedicated propulsion group arrangement has an advantage over the other two configurations since their propulsion system is compromised between low-speed and high-speed flight.

It should be noted that the current research is still developing, thus influences such as payload power consumption were not considered in order to demonstrate the aerodynamic impact in a clear fashion. Besides, there are several future improvements planned.

While the groundwork done for this paper offers great results for preliminary aerodynamic design of UAVs there is room for improvements. Notably one of the biggest improvements would be incorporating the aforementioned QOPTIMIZER in the design loop. This would allow the user to get the best motor prop combination for maximum

efficiency of the propulsion drivetrain. Another improvements that falls inline with the addition of QOPTIMIZER is linking its outputs to the mass module to allow for more accurate representation of the masses of the ESCs and motors. As previously explained the mass being the main driver is this optimization loop, the increase in the fidelity of the mass model would bridge the gap between the final UAV mass from the optimization tool and the actual mass of the UAV if it was to be built. This requires more effort and can be done by performing CAD models of the UAVs and validating the mass of each of the components and then adjusting the models.

The structural model can also be improved by allowing more flexibility in the wing structure configuration (e.g more than one spar, different combination of spars, different lengths). But also a more complex dynamic analysis taking into account aeroelasticity modelling could be included.

The aerodynamic model could be improved to include more of the aircraft configuration body parts in the drag calculations to be better representative of the actual in flight conditions. Finally adding an analysis of the transition phase from VTOL to cruise and ensuring the stability and the success of the transition would be a very valuable addition to the tool assuring the user that the UAV would be able to accomplish the whole flight mission.

Acknowledgments

The authors would like to express gratitude to the funding support from Delair and ANRT (Association nationale de la recherche et de la technologie), and the technical inputs from Delair in consolidating model assumptions and operational conditions.

References

- [1] Binz, F., Islam, T., and Moormann, D., "Attitude control of tiltwing aircraft using a wing-fixed coordinate system and incremental nonlinear dynamic inversion," *International Journal of Micro Air Vehicles*, Vol. 11, 2019, p. 1756829319861370. <https://doi.org/10.1177/1756829319861370>, URL <https://doi.org/10.1177/1756829319861370>.
- [2] Lustosa, L. R., Defajé, F., and Moschetta, J.-M., "Development of the flight model of a tilt-body MAV," International Micro Air Vehicle Conference and Competition, Toulouse, France, 2014.
- [3] Bronz, M., Smeur, E. J., Garcia de Marina, H., and Hattenberger, G., "Development of a Fixed-Wing mini UAV with Transitioning Flight Capability," 35th AIAA Applied Aerodynamics Conference, AIAA AVIATION Forum, Atlanta, United States, 2017.
- [4] McCormick, B., *Aerodynamics, Aeronautics, and Flight Mechanics*, Wiley, 1994. URL <https://books.google.fr/books?id=ALRkQgAACAAJ>.
- [5] Gray, J. S., Hwang, J. T., Martins, J. R. R. A., Moore, K. T., and Naylor, B. A., "OpenMDAO: An open-source framework for multidisciplinary design, analysis, and optimization," *Structural and Multidisciplinary Optimization*, Vol. 59, No. 4, 2019, pp. 1075–1104. <https://doi.org/10.1007/s00158-019-02211-z>.
- [6] Papageorgiou, A., Tarkian, M., Amadori, K., and Ölvander, J., "Multidisciplinary Design Optimization of Aerial Vehicles: A Review of Recent Advancements," *International Journal of Aerospace Engineering*, Vol. 2018, 2018, p. 21.
- [7] Albuquerque, P. F., Gamboa, P. V., and Silvestre, M. A., "Mission-Based Multidisciplinary Aircraft Design Optimization Methodology Tailored for Adaptive Technologies," *Journal of aircraft*, Vol. 55, No. 2, 2018.
- [8] LENG, Y., "Aerodynamic Design of Long Endurance Convertible UAV," Ph.D. thesis, Institut Supérieur De L'aéronautique Et De L'espace, 10 Avenue Edouard Belin, 31055 Toulouse, 12 2020. An optional note.
- [9] Goates, J. T., "Development of an Improved Low-Order Model for Propeller-Wing Interactions," 2018.
- [10] Leng, Y., Jardin, T., Bronz, M., and Moschetta, J.-M., "Experimental Analysis of a Blown-Wing Configuration during Transition Flight," *AIAA Scitech 2020 Forum*, 2020, p. 1983.
- [11] Biczyski, M., Sehab, R., Whidborne, J., Krebs, G., and Luk, P., "Multirotor Sizing Methodology with Flight Time Estimation," *Journal of Advanced Transportation*, 2020.
- [12] Bronz, M., Moschetta, J.-M., and Hattenberger, G., "Multi-Point Optimisation of a Propulsion Set as Applied to a Multi-Tasking MAV," *International Micro Aerial Vehicle Conference and Competition*, 2012.
- [13] Gatti, M., "Complete preliminary design methodology for electric multirotor," *Journal of Aerospace Engineering*, Vol. 30, No. 5, 2017, p. 04017046.
- [14] Bershinsky, D., Haviland, S., and Johnson, E. N., "Electric multirotor UAV propulsion system sizing for performance prediction and design optimization," *57th AIAA/ASCE/AHS/ASC Structures, Structural Dynamics, and Materials Conference*, 2016, p. 0581.
- [15] "RASA propeller catalogue," <http://3fhobbyservice.jetshop.se/propellrar/rasa-c-247-1.aspx>, 2020. Accessed: 2020-10-30.
- [16] Parenteau, M., Sermeus, K., and Laurendeau, E., "VLM Coupled with 2.5 D RANS Sectional Data for High-Lift Design," *2018 AIAA Aerospace Sciences Meeting*, 2018, p. 1049.
- [17] Phillips, W. F., *Mechanics of flight*, John Wiley & Sons, 2004.
- [18] Sheldahl, R. E., and Klimas, P. C., "Aerodynamic characteristics of seven symmetrical airfoil sections through 180-degree angle of attack for use in aerodynamic analysis of vertical axis wind turbines," 1981. <https://doi.org/10.2172/6548367>.
- [19] Hoerner, S., *Fluid-dynamic drag: practical information on aerodynamic drag and hydrodynamic resistance*, Hoerner Fluid Dynamics, 2001.
- [20] Bianchini, A., Balduzzi, F., Rainbird, J. M., Peiro, J., Graham, J. M. R., Ferrara, G., and Ferrari, L., "An Experimental and Numerical Assessment of Airfoil Polars for Use in Darrieus Wind Turbines—Part II: Post-stall Data Extrapolation Methods," *Journal of Engineering for Gas Turbines and Power*, Vol. 138, No. 3, 2016, p. 032603.
- [21] Leishman, G. J., *Principles of helicopter aerodynamics with CD extra*, Cambridge university press, 2006.

- [22] Murat Leng, Y., Moschetta, J.-M., Jardin, T., and Bronz, “An Analytical Model for Propeller Aerodynamic Efforts at High Incidence,” *54th 3AF International Conference on Applied Aerodynamics, Paris*, 2019.
- [23] Bauknecht, A., Merz, C. B., Raffel, M., Landolt, A., and Meier, A. H., “Blade-tip vortex detection in maneuvering flight using the background-oriented schlieren technique,” *Journal of Aircraft*, Vol. 51, No. 6, 2014, pp. 2005–2014.
- [24] Johnson, W., *Helicopter theory*, Courier Corporation, 2012.
- [25] Lambe, A. B., and Martins, J. R. R. A., “Extensions to the Design Structure Matrix for the Description of Multidisciplinary Design, Analysis, and Optimization Processes,” *9th World Congress on Structural and Multidisciplinary Optimization*, 2012.
- [26] EJ, C., JE, D., PD, F., RM, L., and GR, S., “Problem formulation for multidisciplinary optimization.” *SIAM Journal on Optimization*, Vol. 4, 1994.
- [27] “Quantum System Tron F90+ Product Page,” <https://www.quantum-systems.com/project/tron-f90/>, 2020. Accessed: 2020-11-28.